MONTE CARLO SIMULATION OF CARRIER TRANSPORT IN $Cd_{1-x}Zn_xTe$

M. AKARSU[a*], S. AYDOGU[b], O. OZBAS[a], S. KARAKAYA[a]
[a]*Eskişehir Osmangazi University , Physics Department, Eskisehir-TURKEY*
[b]*Dumlupınar University, Physics Department, Kütahya, TURKEY*

Field dependent drift velocity results are presented for carrier transport in $Cd_{1-x}Zn_xTe$ material based on a Monte Carlo model. Scattering mechanisms considered in the simulations are ionized impurity, polar optical phonon, acoustic phonon, non-polar optical phonon, intervalley, dislocation and alloy scattering. The electron energy, steady-state drift velocity and band occupancy are calculated as a function of electric field for different alloy compositions. The dependence of the relevant transport properties on the parameters is discussed. Low–field drift mobilities are extracted from the velocity-field curves. The material could be useful and developed as transparent conductors for solar energy applications.

(Received May 5, 2011; accepted May 21, 2011)

Keywords: CdZnTe, Monte Carlo, Drift velocity, Drift mobility, Carrier transport

1. Introduction

The II-VI semiconductor compounds CdTe, ZnTe and their alloys $Cd_{1-x}Zn_xTe$ have important applications such as infrared detectors, solar cell and other devices [1-3]. The room temperature band gap of these materials can be tuned from 1.61 eV in CdTe to 2.26 eV in ZnTe by controlling the alloy composition. The large band gap of the solar cells is either used in fluorescent plastic concentrator or in high-efficiency thin films in tandem solar cells. High efficiency solar cells can be attained by the development of two junctions one stacked on top of each other into tandem structures. So that, if a photon is not able to excite an electron-hole pair in the top cell can create a pair in the bottom cell, which has a smaller band gap. For a two junction tandem device structure, the band gap of the top cell should be 1.6-1.8 eV and for the bottom cell should be 1 eV to reach efficiencies in the range of 25% [4,5]. Cadmium Zinc Telluride which has a tunable band gap of 1.61-2.26 eV is a candidate for the top cell of the tandem structure [6,7]. In this work we apply the Monte Carlo method to study steady-state electron transport in CdTe, ZnTe and their alloys $Cd_{1-x}Zn_xTe$ as a function of temperatures and electric field using recently determined material parameters. Effects of dislocations on the low-field electron mobilities are studied.

2. Model description

The Monte Carlo method is often used in novel device simulations. It provides a useful tool for the development, analysis, and understanding of semiconductor devices. The single particle Monte Carlo method, as applied to charge transport in semiconductors, consist of a simulation of the motion of one electron inside the crystal, subject to the action of external forces due to applied electric field and of given scattering mechanisms [8,9]. The principal input for the Monte Carlo method used in the transport calculations is the band structure description of the semiconductor material. A nonparabolic three-valley model for the conduction band is employed CdZnTe. The nanparabolicity being treated through the application of the following form [10]:

* *Corresponding author: makarsu@ogu.edu.tr

$$\frac{\hbar^2 k^2}{2m^*} = \gamma(E) = E(1+\alpha E)$$
$$\alpha = \frac{1}{E_g}\left(1-\frac{m^*}{m_0}\right)^2 \quad (1)$$

where $\hbar$ is the reduced Planck constant, k is the wave vector, E is the electron energy relative to the bottom of valleys, m^* is the effective mass at the band edge, m_0 is free electron mass and E_g is the energy gap of semiconductor.

The scattering rate due to the polar optical phonon is given by [10]:

$$\lambda_o(k) = \frac{em^{*1/2}\omega_0}{\sqrt{2}\hbar}\left(\frac{1}{\varepsilon_\infty}-\frac{1}{\varepsilon_s}\right)\frac{(1+2\alpha E')}{\gamma^{1/2}(E)}F_0(E,E')\times\begin{Bmatrix} N_0 & \text{(absorption)} \\ (N_0+1) & \text{(emission)}\end{Bmatrix} \quad (2)$$

Where

$$E' = \begin{Bmatrix} E+\hbar\omega_0 & \text{(absorption)} \\ E-\hbar\omega_0 & \text{(emission)}\end{Bmatrix}$$

and

$$F_0(E,E') = C^{-1}\left(A\ \ln\left|\frac{\gamma^{1/2}(E)+\gamma^{1/2}(E')}{\gamma^{1/2}(E)-\gamma^{1/2}(E')}\right| + B\right)$$
$$A = [2(1+\alpha E)(1+\alpha E')+\alpha\{\gamma(E)+\gamma(E')\}]^2$$
$$B = -2\alpha\gamma^{1/2}(E)\gamma^{1/2}(E')[4(1+\alpha E)(1+\alpha E')+\alpha\{\gamma(E)+\gamma(E')\}]$$
$$C = 4(1+\alpha E)(1+\alpha E')(1+2\alpha E)(1+2\alpha E')$$
$$N_0 = \left[\exp\left(\hbar\omega_0/k_B T_L - 1\right)\right]^{-1}.$$

$\gamma(E)$ is defined by Equation (1), and ω_0 is the optical-phonon frequency. N_0 is the polar optical phonon occupation number, and T_L is the lattice temperature. For high-energy electrons, the scattering rate is not strongly dependent on the electron energy. It should be also noted that a threshold energy $\hbar\omega_0$ exist for the phonon emission process.

The scattering rate for the acoustic phonon scattering is given by [10]:

$$\lambda_a(k) = \frac{(2m^*)^{3/2}k_B T_L \Xi_d^2}{2\pi\rho s^2\hbar^4}\gamma^{1/2}(E)(1+2\alpha E)F_a(E) \quad (3)$$

where

$$F_a(E) = \frac{(1+\alpha E)^2+\frac{1}{3}(\alpha E)^2}{(1+2\alpha E)^2}$$

ρ is the density of material, s is the velocity of longitudinal elastic waves and Ξ_d is the deformation potential. The acoustic phonon scattering rate increases with the increase of the electron energy because it depends on the density of states that increases with electron energy.

The scattering rate due to the ionized impurity scattering is given by [10]

$$\lambda_i(k) = \frac{2\sqrt{2}\pi n e^4 m^{*1/2}}{\varepsilon_0^2\hbar^2\beta^2}\frac{(1+2\alpha E)}{[E(1+\alpha E)]^{1/2}} \quad (4)$$

where β is the inverse of screening length and related to the electron concentration n by

$$\beta^2 = \frac{4\pi n e^2}{\varepsilon_0 k_B T_L}$$

Alloy scattering rate is given by [11,12]

$$\lambda_{al}(k) = \frac{3\sqrt{2}\pi x(1-x)\Xi_{al}^2[(m_\perp^*)^2 m_\parallel^*]^{3/2}}{16\pi\hbar^4}\sqrt{(E(1+2\alpha E))(1+2\alpha E)\left(a_k^2+\frac{c_k^2}{3}\right)}$$

(5)

where

$$a_k = \left[\frac{1+\alpha E}{1+2\alpha E}\right]^{1/2} \quad ; \quad c_k = \left[\frac{\alpha E}{1+2\alpha E}\right]^{1/2}$$

Ξ_{al} is the alloy deformation potential, x is the alloy composition and n_c is the cation density.s
Dislocation scattering rate is given by [13]

$$\lambda_{dis}(k) = \frac{N_d m^* e^4}{\hbar^3 \varepsilon_s^2 c^2} \frac{\lambda^4}{(1+4\lambda^2 k_\perp^2)^{3/2}} \tag{6}$$

where N_d is the dislocation density, $k_\perp$ is the component of electron wave vector k perpendicular to the direction of the dislocation and λ is the Debye Length, defined as

$$\lambda = \left(\varepsilon_0 k_B T_e / n e^2\right)^{1/2}.$$

The dislocation scattering is an elastic interaction without loss or gain of energy, and the effect of the dislocation direction on the mobility was neglected in the simulation.

3. Results and discussion

Electron transport properties of $Cd_{1-x}Zn_xTe$ were studied using the single particle Monte Carlo method in the simulation time of 2 ns. Material parameters used in the calculations, were given in Table 1, have been taken from [14-21]. The scattering mechanisms we considered in our Monte Carlo simulation include ionized impurity, polar optical phonon, acoustic phonon, nonpolar optical phonon, intervalley, alloy and dislocation scattering in a nonparabolic band. Alloy deformation potential has been taken from Suzuki [21] as 0.78 eV. Figure 1 shows the steady-state electron drift velocity in $Cd_{1-x}Zn_xTe$ calculated as a function of the applied electric field strength at a crystal temperature of 300 K for a dislocation density of $1x10^9$ cm^{-2}. Nearly linear increase in drift velocity of CdTe with the applied electric field up to 12 kV/cm was found. At this electric field value, electron drift velocity reached a peak value of $1.3x10^7$ cm/s. Any further increase of the electric field strength results in reduced drift velocity. This effect is known as the negative differential conductivity in CdTe [14,15]. It is due to the transfer of electrons from the Γ-valley, where they have small effective mass, to the L-valley, where they have a larger effective mass, which were predicted by Borsari [16].

Table 1. Parameters used in the Monte Carlo calculations (extracted from [14-21]).

Parameters	CdTe	ZnTe
Band gap (eV)	1.611	2.263
Γ-L Energy separation $\Delta E_{\Gamma\text{-}L}$ (eV)	1.502	1.890
Effective mass at Γ (m^*/m_0)	0.092	0.154
Effective mass at L (m^*/m_0)	0.72	0.80
Material density (g/cm^3)	5.75	5.72
Static dielectric constant ($\varepsilon_s/\varepsilon_0$)	10.5	9.67
High frequency dielectric constant ($\varepsilon_\infty/\varepsilon_0$)	7.2	7.28
Longitudinal sound velocity (m/s)	3370	3904
Acoustic deformation potential (eV)	9.5	7.76
Optical phonon energy (meV)	20.82	26.1
Intervalley optical phonon energy (meV)	17.35	20.3
Intervalley deformation potential (eV/m)	$4.7x10^{10}$	$3.5x10^{10}$

Electron drift velocity in CdTe for the 12 kV/cm electric field value was reported by Borsari as 1.4×10^7 cm/s at 300 K. Electron drift velocity in ZnTe reached a peak value of 1.2×10^7 cm/s at the electric field of 22 kV/cm. The simulation shows that the dominant scattering mechanisms under low-electric field strength are ionized impurity, polar optical phonon and acoustic phonon scattering. The relative importances of ionized impurity and acoustic phonon scattering decrease with electric field strength, while polar optical phonon scattering becomes the dominant scattering mechanism above 12 kV/cm for CdTe and 22 kV/cm for ZnTe. Under high field conditions, electrons have higher energy. Polar optical phonon and intervalley phonon scatterings become most probable. The dependence of the velocity-field relationship on increasing Zn mole fraction in $Cd_{1-x}Zn_xTe$ arises mainly from increases in the band gap, the Γ-L separation and effective mass. The increasing electron effective mass, in the central valley, with increasing Zn mole fraction results in decreasing low-field mobility. With increasing Zn mole fraction the Γ-L valley separation increases with a consequent increase in the critical electric field, defined as the electric field where the velocity peaks.

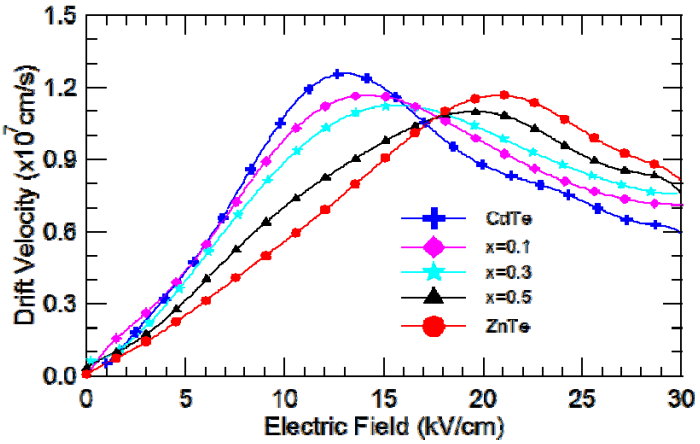

Fig. 1. Electron drift velocity as a function of the electric field calculated for $Cd_{1-x}Zn_xTe$ with varying Zn mole fraction at 300 K and $N_d=1x10^9$ cm^{-2} dislocation concentration.

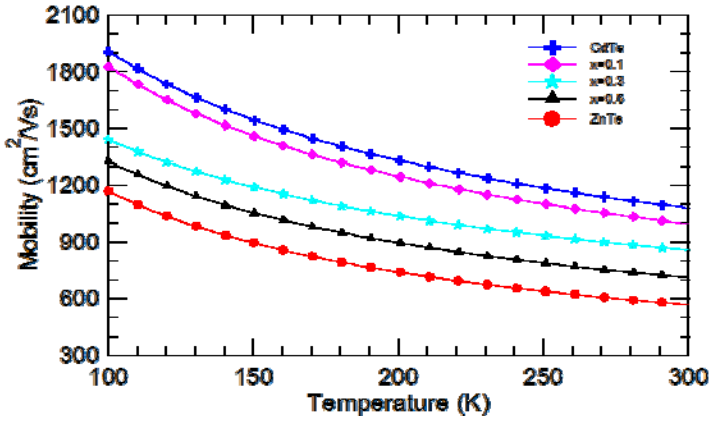

Fig. 2. Calculated electron mobilities in $Cd_{1-x}Zn_xTe$ as a function of the lattice temperature at the 10 kV/cm electric field strength and $N_d=1x10^9$ cm^{-2} dislocation concentration.

The increase in Γ-L separation with increasing Zn mole fraction also results in a reduction in the intervalley scattering rate with a consequent decrease in the population in the upper valley and higher drift velocity at high fields. The numerically calculated electron mobility is shown in Figure 2 as a function of the temperature for various Zn mole fractions at 10 kV/cm electric field strength and $1x10^9$ cm^{-2} dislocation density. A room temperature mobility of 1100 cm^2/Vs and 600 cm^2/Vs are obtained for CdTe and ZnTe respectively. It is reported in Suzuki [21] as 950 cm^2/Vs and in Yadong [22] as 1000 cm^2/Vs for CdTe at 300 K. Figure 2 clearly shows that, with increasing the Zn mole fraction, the low field mobility decreases with the temperature. The effect of structural defects on the low-field electron mobility in CdTe and ZnTe at 300 K is shown in Figure 3 as a function of the dislocation concentration. The ionized impurity concentration was set to be $1x10^{17}$ cm^{-3} in the simulation. In Figure 3, as the dislocation density exceeds $N_d = 10^{10}$ cm^{-2}, the low field mobility starts to decrease. In the range of $N_d = 10^{10}$-10^{12} cm^{-2}, the room-temperature mobilities is strongly dependent on the dislocation density with a decrease from 1100 cm^2/Vs at 10^{10} cm^{-2} to 700 cm^2/Vs at 10^{12} cm^{-2} for CdTe and 580 cm^2/Vs at 10^{10} cm^{-2} to 300 cm^2/Vs at 10^{12} cm^{-2} for ZnTe.

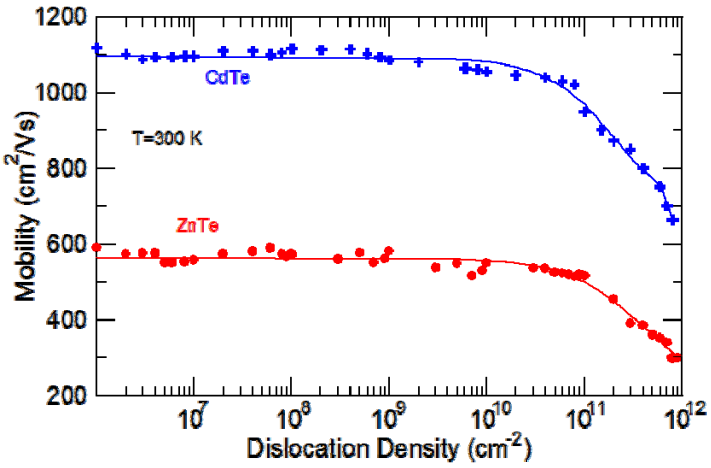

Fig. 3. Mobility in CdTe and ZnTe for various dislocation concentrations at 300 K.

4. Conclusions

Monte Carlo simulation results show that ionized impurity and acoustic phonon scattering are the dominant mechanisms at low electric field. Polar optical phonon scattering becomes important at high electric field and high temperature. The low-field electron mobility in CdTe and ZnTe decreases drastically for $N_d = 10^{10}$-10^{12} cm^{-2} as the dislocation density increase at room temperature. For low dislocation densities, the room temperature mobility does not depend on N_d.

References

[1] A. Arbaoui, A. Outzourhit, N. Achargui, H. Bellakhder, E.L. Ameziane, J.C. Bernede, Solar Energy Materials and Solar Cells, **90**, 1364–1370 (2006).
[2] K. Prabakar, S. Venkatachalam, Y.L. Jeyachandran, S.K. Narayandass, D. Mangalaraj, Solar Energy Materials and Solar Cells, **81**, 1–12 (2004).
[3] D.K. Dwivedi, Dayashakar, Maheshwar Dubey, Chalcog. Lett., **6**(7), 315 (2009).
[4] Gowri Sivaraman, "Characterization Cadmium Zinc Telluride Solar Cells", Masters Thesis,

University of South Florida, (2003).
[5] Senthilnathan Subramanian, "Characterization of Cadmium Zinc Telluride Solar Cells by RF Sputtering", Masters Thesis, University of South Florida, (2004).
[6] M. Becerril, H. S. Lopez, O. Z. Angel, Rev. Mexicana De Fisica, **50** (6) 588-593, (2004).
[7] R. Dhere, T. Gessert, J. Zhou, S. Asher, J. Pankow and H. Moutinho, Investigation of CdZnTe for Thin-Film Tandem Solar Cell Applications, Materials Research Society Spring Meeting, San Fransisco, California, April 21-25 (2003).
[8] O. Ozbaş, M. Akarsu, Turk. J. Phys. **26**, 283 (2002).
[9] M. Akarsu, O. Ozbas, *Math.& Comp. Appl.*, **10**, (1), 19 (2005).
[10] W. Fawcett, A. D. Boardman, and S. Swain, J. Phys. Chem. Solids, 31, 1963 (1970).
[11] M. Akarsu, Determination of transport properties in Hg doped CdTe semiconductor compound by Monte Carlo simulation, Ph. D. Thesis, Department of Physics, Science Institute of Eskisehir Osmangazi University, Eskisehir, Turkey, (2003).
[12] Vincent W.L. Chin, R.J. Egan, and T.L. Tansley, J. Appl. Phys. **69** (6), 3571 (1991).
[13] Xin-Gang Yu and Xin-Gang Liang, J. Appl. Phys. **103**, 043707 (2008).
[14] M. Akarsu, O, Ozbaş, Balkan Physics Letters, 12 (1), pp.38-45 (2004).
[15] C. Jacoboni and L. Reggiani, Physics Letters, Vol. **33A**, No. 6, 333 (1970).
[16] V. Borsari and C. Jacoboni, Phys. Stat. Sol. (b), 54, 649 (1972).
[17] D. Kranzer, J.Phys. C: Solid State Phys.,Vol. **6**, (1973).
[18] N. Bouarissa, Physica B **399**, 126-131 (2007).
[19] J. E. Toney, T. E. Schlesinger, R. B. James, Nuc. Ins. and Meth. in Phys. Res. A **428**, 14-24 (1999).
[20] K. Suzuki, S. Seto, T. Sawada, K. Imai, IEEE Trans. Nuc. Sci., **49**(3), 1287 (2002).
[21] K. Suzuki, S. Seto, A. Iwata, M. Bingo, T. Sawada and K. Imai, Jour. of Elect. Mat., **29**(6), 704 (2000).
[22] X. Yadong, X. Lingyan, W. Tao, Z. Gangqiang, F. Li, J. Wanqi, Sellin P, Jour. of Semic., **30**(8), (2009).